A Robust Structure-Adaptive Hybrid Vector Filter for Color Image Restoration

Zhonghua Ma, *Member, IEEE*, Hong Ren Wu, and Bin Qiu, *Senior Member, IEEE*

***Abstract*—A robust structure-adaptive hybrid vector filter is proposed for digital color image restoration in this paper. At each pixel location, the image vector (i.e., pixel) is first classified into several different signal activity categories by applying a modified quadtree decomposition to luminance component (image) of the input color image. A weight-adaptive vector filtering operation with an optimal window is then activated to achieve the best tradeoff between noise suppression and detail preservation. Through extensive simulation experiments conducted using a wide range of test color images, the filter has demonstrated superior performance to that of a number of well known benchmark techniques, in terms of both standard objective measurements and perceived image quality, in suppressing several distinct types of noise commonly considered in color image restoration, including Gaussian noise, impulse noise, and mixed noise.**

***Index Terms*—Adaptive vector filtering, digital color image restoration, modified quadtree decomposition, structure-adaptive hybrid vector filter.**

I. Introduction

FOR OVER a decade, the vector filtering technique based on multivariate order statistics [1]–[3] has become increasingly popular for color image restoration. The most well known vector filters include the vector median filters (VMF) [4], the vector directional filter (VDF) [5], and the directional-distance filter (DDF) [6]. Adaptive vector filtering techniques [7]–[9] have been developed to deal with variations of color image characteristics and noise distribution. Fuzzy restoration techniques [10], [11] have also been reported demonstrating robust performance for restoration of digital color images corrupted by different types of random noise.

Hybrid vector filtering techniques, such as the adaptive hybrid multivariate filter (AMF) [12], the hybrid directional filter (HF)/the adaptive hybrid directional filter (AHF) [13], and the vector median-rational hybrid filters (VMRHF) [14], have been advanced as a robust solution to suppression of different types of noise corrupting color images. However, these hybrid vector filters have very limited capabilities in structure adaption. For instance, they are often implemented with a fixed filtering window dimension (e.g., 3×3 or 5×5) to restore image structures of varying scales. It is well known that the human visual system perceives image degradations very differently, depending upon whether they are close to or far away from image details/structures [12], [15]. Human eyes are quite sensitive to even a very small amount of noise in flat areas, while they can tolerate a large amount of noise in the neighborhood of an edge. Therefore, structure and window adaptation is essential to the hybrid vector filter design, which enables the filter to use a larger processing window (i.e., a larger group of stochastic samples) in the flat areas to yield sufficient chromatic smoothness, whilst to reduce the processing window size around image details/structures to achieve better image preservation.

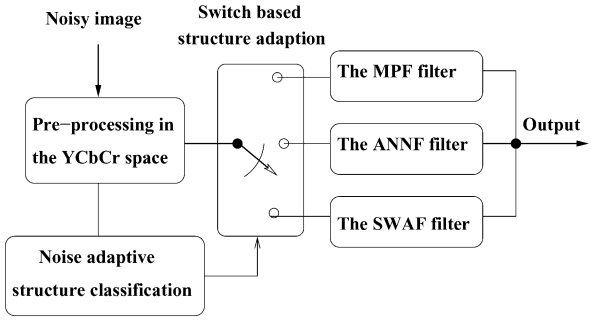

Fig. 1. Schematic diagram of the *structure-adaptive hybrid vector filter*.

In this paper, a robust structure-adaptive hybrid vector filter (SAHVF) is proposed for color image restoration. At each pixel location, the corrupted image vector (pixel) is first classified into several different signal activity categories by noise-adaptive preprocessing and modified quadtree decomposition. For each pixel, a window-adaptive hybrid filtering operation is then activated according to its structure classification. As its processing window dimension and filtering structure can adapt to the local structures and local statistics, respectively, the proposed vector filter is able to achieve better performance in noise suppression, detail preservation, and chromaticity retention than that of the aforementioned classic hybrid vector filters, where different types of noise contamination are encountered. Fig. 1 shows the schematic diagram of the SAHVF filter.

The organization of this paper is as follows. Section II presents statistic models of different types of noise, which often occur in digital color images. Sections III and IV address the noise-adaptive preprocessing and the structure activity classification, respectively. Section V discusses the hybrid

Manuscript received January 20, 2004; revised July 30, 2004. This work was supported by the Australia Research Council under Grant DP0208790. The associate editor coordinating the review of this manuscript and approving it for publication was Dr. M. Schmitt.

Z. Ma was with School of Computer Science and Software Engineering, Monash University, Melbourne, Australia. He is now with School of Information Technologies, University of Sydney, Sydney, Australia (e-mail: frankma@it.usyd.edu.au).

H. R. Wu was with the School of Computer Science and Software Engineering, Monash University, Melbourne, Australia. He is now with the School of Electrical and Computer Engineering, Royal Melbourne Institute of Technology, Melbourne, Australia (e-mail: henry.wu@rmit.edu.au).

B. Qiu is with the School of Computer Science and Software Engineering, Monash University, Melbourne, Australia (e-mail: bq@csse.monash.edu.au).

Digital Object Identifier 10.1109/TIP.2005.857269

vector filtering structure and window adaption tailored for different structure activity classifications. Experimental results are presented in Section VI. Finally, conclusions are drawn in Section VII.

II. Statistic Models of Noises in Digital Color Images

Color images can be contaminated by various types of noise. Nevertheless, the noise models frequently reported in digital image restoration literature are the *impulse noise*, which is of either fixed or random value, the *additive noise* with a zero mean Gaussian or other distributions, and the *mixed noise* as a combination of the impulse and the additive noise.

A. Impulse Noise

Impulse noise often occurs in digital image recording or transmission process as a result of photo-electronic sensor faults or channel bit errors [16], [17]. The intensity of image corruption by the impulse noise is often measured by the noise ratio, which represents the percentage of image pixels corrupted by the impulse noise. Let $\mathbf{C} \equiv \{\mathbf{c} = (c_1, c_2) \,|\, 1 \le c_1 \le H, 1 \le c_2 \le W\}$ denote the pixel coordinates of a color image, where H and W are the height and the width of the image, respectively. At each pixel coordinate $\mathbf{c} \in \mathbf{C}$, a multivariate value $\mathbf{x}(\mathbf{c}) = [x_R(\mathbf{c}), x_G(\mathbf{c}), x_B(\mathbf{c})]^T$ is used to represent input RGB values at the current position. The impulse noise corruption of RGB color image can be expressed by a multivariance model [5], [6]

$$\mathbf{x}(\mathbf{c}) = \begin{cases} \mathbf{s}(\mathbf{c}), & \text{with probability } (1 - p_I) \\ \mathbf{n}_I(\mathbf{c}), & \text{with probability } p_I \end{cases} \tag{1}$$

where $\mathbf{s}(\mathbf{c})$ and $\mathbf{x}(\mathbf{c})$ represent the original and the observed pixel values at coordinate $\mathbf{c}$, respectively, and p_I is the impulse noise ratio. The value of $\mathbf{n}_I(\mathbf{c})$ is generated by substituting at least one color component of the pixel $\mathbf{s}(\mathbf{c})$ by a distinct value d. If d equals the maximum or the minimum value of the digital image (e.g., 255 or 0 for an 8-bit channel of 24-bit RGB color images), the impulse noise is referred to as pepper-and-salt (PS) impulse. A more generalized impulse noise model was also proposed in the literature [5], [17], where impulse values vary between 0 and 255, following a specific statistical distribution (e.g., uniform distribution).

A color channel correlation technique is often used to simulate the impulse corruption in natural color images [5]. First, each RGB channel of image pixels is independently corrupted by the impulse noise with a uniform distribution between [0, 255] and a selected noise ratio (e.g., 10%). Thereafter, a factor $\rho = 0.5$ is used to simulate the error correlation between color components of the corrupted pixel, that is, for each pixel value, if any of other two R/G/B channels has been corrupted by the impulse noise, the current channel will likely suffer a further corruption with a probability of 50%.

B. Additive Noise

The thermal effect of various electronic circuits and the random photon-fluctuation of photo-electronic sensors [16], [17] induce additive noise in digital color images. A generalized model for color images contaminated by the additive noise is given by [12], [16], [17]

$$\mathbf{x}(\mathbf{c}) = \mathbf{s}(\mathbf{c}) + \mathbf{n}_A(\mathbf{c}) \tag{2}$$

where $\mathbf{s}(\mathbf{c})$ and $\mathbf{n}_A(\mathbf{c})$ represent the original pixel value and a multivariate additive noise value at pixel coordinate $\mathbf{c}$, respectively. Without losing generality, it is assumed that the additive noise is introduced in each of RGB channels independently, with a zero mean and the same standard deviation in each channel [16], [17].

The additive noise in natural color images is often modeled as multivariate *Gaussian* noise, whose probability density function (PDF) is given by

$$p[\mathbf{n}_A(\mathbf{c})] = \frac{1}{(2\pi\sigma^2)^{3/2}} \exp\left[-\frac{\|\mathbf{n}_A(\mathbf{c})\|^2}{2\sigma^2}\right] \tag{3}$$

where σ is the standard deviation of the noise in each R/G/B channel and $\|\cdot\|$ represents the L_2 norm.

Additive noise scenarios other than *Gaussian* noise are often used to evaluate the robustness of restoration techniques [17], [18], which include the long-tailed *Laplacian* noise and the short-tailed *uniform* noise. The PDF of the multivariate *Laplacian* noise is given by

$$p[\mathbf{n}_A(\mathbf{c})] = \frac{1}{(2\sigma^2)^{3/2}} \exp\left[-\sqrt{\frac{2}{\sigma^2}}|\mathbf{n}_A(\mathbf{c})|\right] \tag{4}$$

where $|\cdot|$ represents the L_1 norm, and the PDF of the multivariate *uniform* noise can be given by

$$p[\mathbf{n}_A(\mathbf{c})] = \begin{cases} 1/(2\sqrt{3}\sigma)^3, & \text{for } \mathbf{n}_A(\mathbf{c}) \in \Omega(\mathbf{n}; \sqrt{3}\sigma) \\ 0, & \text{else} \end{cases} \tag{5}$$

where $\Omega(\mathbf{n}; \sqrt{3}\sigma)$ represents a cube space defined by $\{\mathbf{n} = [n_1, n_2, n_3]^T; |n_i| \le \sqrt{3}\sigma, i = 1, 2, 3\}$, and σ is the standard deviation of the noise in each R/G/B channel.

C. Mixed Noise

In many situations, color images suffer from both sensor faults and transmission noise [17]. Such scenarios can be described as a *mixed* noise contamination. A generalized model for the *mixed* noise contamination has been given by [12], [17]

$$\mathbf{x}(\mathbf{c}) = \begin{cases} \mathbf{s}(\mathbf{c}) + \mathbf{n}_A(\mathbf{c}), & \text{with probability } (1 - p_I) \\ \mathbf{n}_I(\mathbf{c}), & \text{with probability } p_I \end{cases} \tag{6}$$

where $\mathbf{n}_A(\mathbf{c})$ denotes a multivariate additive noise as in (2), $\mathbf{n}_I(\mathbf{c})$ is an impulse corrupted value as defined in (1), and p_I is the noise ratio to control the occurrence between additive noise contamination and impulse noise corruption. Image corruption by the *mixed* noise has been recognized as one of the most challenging cases for color image restoration [17].

III. Noise-Adaptive Preprocessing

Classic local statistics filters [15], [19] have been used in monochrome image enhancement for decades. They were able to recover primary ergodic image structures from zero mean

additive noise contamination, while keeping high-frequency image details and structures untouched. An efficient way to use local statistics filters in the RGB color space is to implement in a scalar filtering structure with a color de-correlation scheme. The Karhunen–Loueve transform (KLT) [20] has been considered as the best de-correlation transform from a theoretical point of view. However, the RGB to YC_bC_r transformation is more popular in digital imaging and video applications for its computation efficiency and color de-correlation performance [16], and is used in this paper.

The proposed noise-adaptive preprocessing is performed in two steps. The additive noise deviation of the input image is first estimated. Then a presmoothing filter based on the Lee's local statistics filter (LLSF) [19] is used to filter each $Y/C_b/C_r$ channel of the input image independently. Thanks to the color de-correlation and the adaptive noise estimation, better noise suppression was achieved by the presmooth filter without introducing extraneous chromatic distortions.

A. Additive Noise Deviation Estimation

A fast deviation estimation method has been proposed in [21] for deviation estimation of the zero mean Gaussian noise in grayscale images. A 3×3 Laplacian mask is used by the method to pick up the additive noise energy from the input image, which is given by

$$\Xi = \begin{bmatrix} 1 & -2 & 1 \\ -2 & 4 & -2 \\ 1 & -2 & 1 \end{bmatrix}. \tag{7}$$

Let $\mathbf{x}(\mathbf{c}) * \Xi$ denote the convolution operation of applying the mask Ξ at the coordinate $\mathbf{c} \in \tilde{\mathbf{C}}$ of an image $\mathbf{X}$, where $\tilde{\mathbf{C}} = \{(c_1, c_2) \,|\, 1 < c_1 < H, 1 < c_2 < W\}$ denotes all the pixel coordinates except four boundaries. The noise deviation is estimated by [21]

$$\hat{\sigma}_n = \sqrt{\frac{\pi}{2}} \frac{1}{6(W-2)(H-2)} \sum_{\mathbf{c} \in \tilde{\mathbf{C}}} |\mathbf{x}(\mathbf{c}) * \Xi| \tag{8}$$

where $|\cdot|$ represents an absolute operator.

However, as Laplacian masks are very sensitive to any large local outlier [16], the method defined by (7) and (8) cannot provide a reliable noise estimation for scenarios other than normal or short-tailed additive noise contaminations, and is valid for grayscale images only. In order to obtain a robust additive noise estimation from complicated noise scenarios such as *mixed* noise contamination, a new three-step noise estimation method is developed in this paper.

1) First, the input color image $\mathbf{X}$ is processed by a standard VMF filter with a 3×3-pixel window to remove extraneous outliers. The resultant image is denoted as $\tilde{\mathbf{X}}$.
2) Then, (8) is applied to each $Y/C_b/C_r$ channel of the resultant image $\tilde{\mathbf{X}}$ to obtain primitive additive noise deviation estimations for each channel, which are denoted as $\{\tilde{\sigma}_{n,i} \,|\, i = 1, 2, 3\}$.
3) The final additive noise deviation values $\{\hat{\sigma}_{n,i} \,|\, i = 1, 2, 3\}$ are calculated from the primitive eviation estimates $\{\tilde{\sigma}_{n,i} \,|\, i = 1, 2, 3\}$ using an approximation function given by

$$\hat{\sigma}_{n,i} = \max\{\kappa \sqrt{\frac{\pi}{18}} \cdot \tilde{\sigma}_{n,i} - \epsilon, 0\}, \quad i = 1, 2, 3 \tag{9}$$

where $\sqrt{(\pi/18)}$ is used to correct the smoothing effect introduced by the 3×3 standard VMF filter,[1] κ and ϵ are, respectively, two empirically determined parameters to compensate the bias from fine image structures. In this paper, we set $\kappa = 1.2$ and $\epsilon = 4.4$.

B. Presmoothing Filter

Let $\mathbf{x}(\mathbf{c}) = [x_1(\mathbf{c}), x_2(\mathbf{c}), x_3(\mathbf{c})]^T$ represents a YC_bC_r pixel value at coordinate $\mathbf{c} \in \mathbf{C}$, and an $N \times N$-pixel square window centered at the coordinate $\mathbf{c}$ is defined as $\mathbf{W}(\mathbf{c})$, where N is a positive odd integer, i.e., $N = 2\xi + 1, \xi \in \mathcal{N}, \mathcal{N}$ being the set of all positive integers. The output of the presmoothing filter, $\hat{\mathbf{x}}(\mathbf{c}) = [\hat{x}_1(\mathbf{c}), \hat{x}_2(\mathbf{c}), \hat{x}_3(\mathbf{c})]^T$, can be given by

$$\hat{x}_i(\mathbf{c}) = \hat{m}_i(\mathbf{c}) + \frac{\hat{\sigma}^2_{x,i}(\mathbf{c})}{\hat{\sigma}^2_i(\mathbf{c})} [x_i(\mathbf{c}) - \hat{m}_i(\mathbf{c})], \quad i = 1, 2, 3 \tag{10}$$

where $\hat{m}_i(\mathbf{c})$ and $\hat{\sigma}^2_i(\mathbf{c})$ are the ensemble local mean and variance at coordinate $\mathbf{c}$ in each $Y/C_b/C_r$ channel, respectively, that is

$$\hat{m}_i(\mathbf{c}) = \frac{1}{N^2} \sum_{\mathbf{c} \in \mathbf{W}(\mathbf{c})} x_i(\mathbf{c}), \quad i = 1, 2, 3 \tag{11}$$

$$\hat{\sigma}^2_i(\mathbf{c}) = \frac{1}{N^2} \sum_{\mathbf{c} \in \mathbf{W}(\mathbf{c})} [x_i(\mathbf{c}) - \hat{m}_i(\mathbf{c})]^2, \quad i = 1, 2, 3 \tag{12}$$

and $\hat{\sigma}^2_{x,i}(\mathbf{c})$ is the ensemble local image signal variance in each $Y/C_b/C_r$ channel. The statistical independence between image signals and the additive noise yields

$$\hat{\sigma}^2_{x,i}(\mathbf{c}) = \max\{\hat{\sigma}^2_i(\mathbf{c}) - \hat{\sigma}^2_{n,i}, 0\} \tag{13}$$

where $\{\hat{\sigma}^2_{n,i}, i = 1, 2, 3\}$ are the contaminated additive noise variances in each $Y/C_b/C_r$ channel of the corrupted image. These values can be robustly estimated from the input noisy color image using the method given in Section III-A, while, in the classic LLSF filter structure [19], such noise variances have to be known *a priori*.

Furthermore, in order to achieve a sufficient suppression of noises in background areas, the window dimension of the presmoothing filter needs to be adaptive to different contaminating noise levels. In this paper, such an adaptation is implemented in a stepwise scheme according to the estimated additive noise deviation value, i.e., the presmoothing filter window is set to 3×3 for low noise deviation ($0 \leq \hat{\sigma}_{n,1} \leq 15$), 5×5 for medium noise deviation ($15 < \hat{\sigma}_{n,1} \leq 30$), and 7×7 for higher noise deviation.

IV. Structure Activity Classification

The purpose of the structure activity classification is to partition the local structures so that a proper filtering structure and dimension can be determined for each pixel position to

[1] It is stated in [22] that, for a group of normal distributed input data, the output variance of a median filter with a window size N is equal to $(\pi/2N)$.

TABLE I
RECOMMENDED VALUE FOR DECOMPOSITION THRESHOLD

Image Detail (*Sample*)	Low (*Lena*)	Middle (*Barbara*)	High (*Mandrill*)
Value of η	2.0	1.0	0.7

achieve the best visual quality. The luminance channel (image) of the preprocessed input color image, which contains most of image structure information, is first decomposed by a modified quadtree decomposition technique. Then, a structure activity index is calculated for each pixel position according to the decomposition results. Classification is finally applied to the activity index of each pixel to partition it into one of three signal activity areas, namely, the *high-activity area*, the *medium-activity area*, and the *low activity area*. Each of them will relate to a well-designed filtering process which provides the optimal restoration solution for the partitioned pixel.

A. Modified Quadtree Decomposition

Denote the luminance of the preprocessed input image as $\mathbf{L}$, the modified quadtree decomposition decomposed the preprocessed input image into nonoverlapping rectangular *homogeneous block*s according to a local dispersion criterion adopted from the variable block truncation coding (VBTC) [23]. The details of the modified quadtree decomposition process are depicted as follows.

1) Starting from the entire image $\mathbf{L}$. The ensemble deviations of four equally divided rectangular blocks are obtained first as $\{v_i \,|\, i = 1, 2, 3, 4\}$. Given a predetermined threshold T, if

$$\max_{1 \le i \le 4} \{v_i\} - \min_{1 \le i \le 4} \{v_i\} \le T \tag{14}$$

the considered block is marked as a *homogeneous block*. Otherwise, further splitting is applied.
2) Repeat the aforementioned splitting step on each divided block independently and recursively, until all the subblocks are either *homogeneous blocks*, or reaching the minimum size of 1×1 pixel.
3) For any *homogeneous block* with its size bigger than 16×16-pixel, split it into four equal-size rectangular blocks directly and recursively, until all the subblocks reach 16×16-pixel in size.

Similar to [24], the threshold T here needs not to be highly accurate as long as the decomposition produces a reasonable number of homogeneous rectangular blocks. In this paper, its value is given by a robust median absolute deviation (MAD) scale estimation on all local ensemble deviations, i.e.,

$$T = \eta \cdot \mathrm{MAD}\{\hat{\sigma}_{3\times 3}(\mathbf{c}) \,|\, \mathbf{c} \in \mathbf{C}\} \tag{15}$$

where $\hat{\sigma}_{3\times 3}(\mathbf{c})$ is the ensemble deviation obtained from a 3×3 local window centered at position $\mathbf{c}$, and η is an empirically determined parameter used to reflect the structure dispersion of the input image. For most corrupted natural color images which we tested, the best value for η was always founded in the range of [0.7, 2.5]. Recommended values of η for different natural color images are presented in Table I.

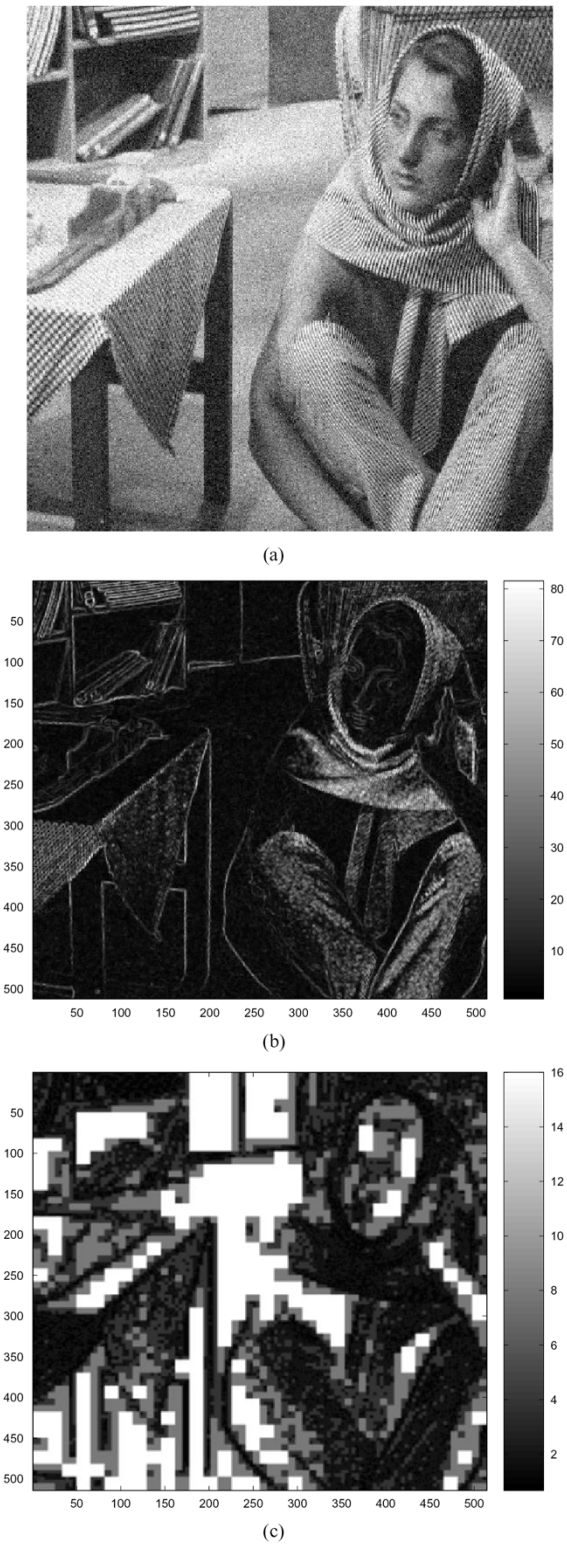

Fig. 2. Result of the modified quadtree decomposition on the corrupted RGB image *Barbara*, where the decomposition threshold $\eta = 1.0$. (a) *Barbara* corrupted by *Gaussian* noise with $\sigma = 30$. (b) Local luma deviations of the preprocessed image, where deviations are mapped into gray scales shown in the bar. (c) The output of decomposition, where *homogeneous block* sizes are mapped into gray scales shown in the bar.

Fig. 2 shows a decomposition example with the RGB image *Barbara* corrupted by *Guassian* noise with deviation $\sigma = 30$, where (a) is the corrupted image, (b) is the luminance local deviations of the corrupted image, and (c) is the decomposition

result. The modified quadtree decomposition has produced satisfactory results, as most of background areas are segmented into big blocks, while fine image structures are decomposed into very small blocks.

B. Structure Activity Partition

The block size from the modified quadtree decomposition has provided an effective structure description for the input image. However, directly using such dyadic size values as the structure activity index may introduce unpleasant block artifacts to the reconstructed image. In this paper, the structure activity index $I(\mathbf{c})$ is calculated as the ensemble mean of the local decomposition results centered at each position $\mathbf{c}$, that is

$$I(\mathbf{c}) = \frac{1}{2L+1} \sum_{\mathbf{c} \in \mathbf{\Phi}(\mathbf{c})} B(\mathbf{c}) \tag{16}$$

where $B(\mathbf{c})$ denotes the decomposed block size at position $\mathbf{c}$ and $\mathbf{\Phi}(\mathbf{c})$ denotes a local area centered at the position $\mathbf{c}$, with its size equal to $2L+1$. A 3×3 local area is used throughout our experiments, where $2L+1 = 9$.

Based on the obtained structure activity index $I(\mathbf{c})$, each observed pixel $\mathbf{x}(\mathbf{c})$ is finally classified into one of the following different structure groups.

1) *High-activity area where* $1.0 \leq I(\mathbf{c}) \leq 2.5$: This group often relates to high-frequency details or impulse noise. In order to preserve fine image structure while suppressing impulse noises, a high nonlinear filter with a small processing window should be employed to detect and restore the original image pixel value.
2) *Medium-activity area where* $2.5 \leq I(\mathbf{c}) < 5.5$: This group usually includes primary image edge structures and textures. Moderate nonlinear filtering will be used to remove possible impulse noise, to smooth the texture area, and to preserve the primary structure. Its processing window should also be adaptive to the different structure distribution.
3) *Low activity area where* $5.5 \leq I(\mathbf{c}) < 16.0$: This is the group related to the flat background area with, possibly, little variance or distortion. In order to favor the human perception without losing computation efficiency, a linear (weighted) filter with a relatively big processing window should be considered to provide sufficient smooth effect for the concerned area.

V. Hybrid Vector Filtering Structure

In order to match the restoration requirements of different structure groups in the previous section, it is proposed here a switch based hybrid-filtering structure with three subadaptive-vector-filters. The three subfilters are the *modified peer filter* (MPF) which is optimal in reducing image degradation in the high-activity areas, the *adaptive nearest neighbor filter* (ANNF) which can effectively remove the noise while preserving the image edge structure in the medium-activity areas, and the *structure weighted average filter* (SWAF) designed to smooth the small distortion in the large low-activity areas. The switching mechanism, as shown in Table II, is implemented according to the structure activity index of each pixel position. Small windows and high-detail preservation nonlinear subfilters are proposed for effective removal of noises contained in image edges and detail areas, while large windows and more linear filtering scheme are proposed for sufficient smoothing of small distortions in flat background areas.

A. Modified Peer Filter

The peer group filter (PGF) was proposed in [25] for image enhancement. It consists of a Fisher discrimination based on the Euclidean distance and a standard Gaussian filter. However, the Euclidean distance cannot precisely reflect the visual similarity between two color image pixels [9]. The Fisher discrimination may malfunction for pixel set consisting of two or more distinct clusters [26], e.g., a sharp edge with impulse noises. The fixed standard Gaussian filter tends to over-smooth fine image details [27]. Therefore, the modified peer filter is formulated here to provide better structure preservation for noise removal in image detail areas. The MPF is distinctively different from the PGF filter in three aspects.

1) A distance function combining the vector magnitude and angle distance similarities is proposed to replace the Euclidean distance for vector distance measure.
2) Instead of treating the pixel which globally maximize the Fisher objective function as the cluster boundary, the pixel related to the first Fisher objective function maximum is treated as the boundary.
3) An *L*-filter structure is proposed for pixel reconstruction. The filter updates its weights according to an aggregated vector distance between the CP and its neighbors.

Given a filtered window centered at $\mathbf{c}$, denote its CP as $\mathbf{x}_0 \equiv \mathbf{x}(\mathbf{c})$, and other pixels of the window as the neighbors of the CP, which are organized in a lexicographic order as $\{\mathbf{x}_1, \mathbf{x}_2, \cdots, \mathbf{x}_{2L}\}$, where $(2L+1)$ is the size of the window. The proposed vector distance measure between the CP and its neighboring pixels is defined based on the normalized vector magnitude and angle similarities [7], i.e.,

$$d_i = 1 - \left[\frac{\mathbf{x}_0 \mathbf{x}_i^T}{||\mathbf{x}_0|| ||\mathbf{x}_i||}\right] \left[\frac{1 - |||\mathbf{x}_0|| - ||\mathbf{x}_i|||}{\max\{||\mathbf{x}_0||, ||\mathbf{x}_i||\}}\right] \quad 1 \leq i \leq 2L \tag{17}$$

The vector distances are then ranked in an ascending order such that $d_{(1)} \leq d_{(2)} \leq \cdots \leq d_{(2L)}$, which implies the same order of the CP's neighboring pixels as $\{\mathbf{x}_{(1)}, \mathbf{x}_{(2)}, \cdots, \mathbf{x}_{(2L)}\}$. Then, the Fisher objective functions [26] are obtained on the basis of these ordered vector distances, i.e.,

$$F(k) = \frac{||m_1 - m_2||}{v_1 + v_2}, \quad k = 1, 2, \cdots, 2L-1 \tag{18}$$

where

$$m_1 = \frac{1}{k} \sum_{i=1}^{k} d_{(i)}, \quad m_2 = \frac{1}{2L-k} \sum_{i=k+1}^{2L} d_{(i)} \tag{19}$$

$$v_1 = \sum_{i=1}^{k} [d_{(i)} - m_1]^2, \quad v_2 = \sum_{i=k+1}^{2L} [d_{(i)} - m_2]^2. \tag{20}$$

TABLE II
STRUCTURE CLASSIFICATION AND THEIR HYBRID FILTERING AND WINDOW ADAPTATION

$I(\mathbf{c})$	1.0– 2.5	2.5–4.0	4.0–5.5	5.5-7.5	7.5-9.5	9.5-16
Classification	*High Active Area*	*Middle Active Area*		*Low Active Area*		
Subfilter	MPF	ANNF		SWAF		
Window size	3×3	3×3	5×5	7×7	9×9	11×11

The neighboring pixel $\mathbf{x}_{(w)}$ with its related Fisher objective functions approaching the first maximum is treated as the boundary of the CP peer group, i.e.,

$$w = \min \arg_k \{F(k)\} \tag{21}$$

where

$$F(k+1) - F(k) \leq 0 \quad \text{and} \quad F(k) - F(k-1) \geq 0. \tag{22}$$

Based on the classified CP peer group $\{\mathbf{x}_{(i)}, i = 1, 2 \cdots, w\}$, the pixel value at position $\mathbf{c}$ is reconstructed by the MPF using a L-filtering structure, i.e.,

$$\mathbf{y}(\mathbf{c}) = \frac{\sum_{i=1}^{w} \alpha_i \mathbf{x}_{(i)}}{\sum_{i=1}^{w} \alpha_i} \tag{23}$$

where $\{\alpha_i, i = 1, 2 \cdots, w\}$ are structure-adaptive weights based on the vector ordered distances $\{d_i, i = 1, \cdots, w\}$, i.e.,

$$\alpha_i = \frac{d_{(w)} - d_{(i)}}{d_{(w)} - d_{(1)}}, \quad i = 1, 2 \cdots, w. \tag{24}$$

B. Adaptive Nearest Neighbor Filter

For the classified medium-activity area, it is desirable to preserve its primary edge structure while applying a strict limitation on local deviations. This task is accomplished by a well defined subfilter: the ANNF proposed by [7]. The window dimension of the ANNF can be 3×3 or 5×5, depending on the structure activity index value of the CP (refer to Table II for details). For a filtering window centered at position $\mathbf{c}$, which covered $(2L+1)$ local pixels $\{\mathbf{x}_0, \mathbf{x}_1, \cdots, \mathbf{x}_{2L}\}$, the output of the ANNF is given by

$$\mathbf{y}(\mathbf{c}) = \frac{\sum_{i=0}^{2L} \beta_i \mathbf{x}_i}{\sum_{i=0}^{2L} \beta_i} \tag{25}$$

where $\{\beta_i, i = 1, \cdots, 2L\}$ are adaptive weights defined as

$$\beta_i = \frac{(D_{\max} - D_i) + \lambda(D_i - D_{\min})}{(1+\lambda)(D_{\max} - D_{\min})}, \quad 0 \leq i \leq 2L \tag{26}$$

with $\{D_i, i = 0, \cdots, 2L\}$ denoting the aggregated normalized vector distances given by

$$D_i = \sum_{j=0}^{2L} \left[\frac{\mathbf{x}_i \mathbf{x}_j^T}{\|\mathbf{x}_i\| \|\mathbf{x}_j\|} \right] \left[1 - \frac{\| \|\mathbf{x}_i\| - \|\mathbf{x}_j\| \|}{\max\{\|\mathbf{x}_i\|, \|\mathbf{x}_j\|\}} \right] \tag{27}$$

and

$$D_{\max} = \max_{0 \leq i \leq 2L} D_i, \quad D_{\min} = \min_{0 \leq i \leq 2L} D_i. \tag{28}$$

The λ in (26) is an empirical parameter used to control the nonlinearity of the weighting measure. A robust choice has been proposed in [7], where $\lambda = (D_{\max} - D_{\min})^{-1}$.

C. Structure Weighted Average Filter

The classified low-activity areas are usually flat areas of the input image with small distortions, or backgrounds containing impulse noises. Classic vector filters such as the ANNF with a large window dimension can be used to provide a sufficient distortion suppression for such areas. However, the computation costs of the ANNF raise dramatically with the increased window dimension. The structure weighted average filter is designed in this paper to effectively suppress of small distortions and noises remaining in low-activity areas, while reducing quite a significant amount of computation overhead.

Denote the current filter window as $\mathbf{W}(\mathbf{c})$, whose dimension is automatically adjust from 7×7 to 11×11 in order to provide sufficient smoothing for each concerned area (refer to Table II for details). The output of the SWAF is calculated using a structure weighted averaging on all the local pixels in the filter window, i.e.,

$$\mathbf{y}(\mathbf{c}) = \frac{\sum_{\mathbf{c} \in \mathbf{W}(\mathbf{c})} I(\mathbf{c}) \mathbf{x}(\mathbf{c})}{\sum_{\mathbf{c} \in \mathbf{W}(\mathbf{c})} I(\mathbf{c})} \tag{29}$$

where $I(\mathbf{c})$ represents the structure activity index at position $\mathbf{c}$ given by (12). Since $I(\mathbf{c})$ is usually small for high-activity areas, such as high-frequency details or impulse noises, but large for smooth areas, such a weighting structure is able to avoid the distortion spreading of impulse noise corruption in flat areas, and to provide a smoother reconstruction for better perceptual image quality.

D. Hybrid Filtering for Impulse Noise Removal

Since impulse noise only corrupt some parts of the image but leave others intact, the implementation of the hybrid filter for impulse noise removal is specially designed to take advantage of such characteristic and to achieve a better structure preservation. In the proposed "impulse noise mode," the presmooth filtering is skipped to best keep the image structure in smooth areas, and the structure activity classification is applied directly to the input noisy image. Reconstruction filtering is only applied to those pixels whose recommended processing window is equal to 3×3 according to Table II, and only the MPF or the ANNF with a 3×3 window are used to recover the image structure from impulse corruption. Other classified pixel areas are left unchanged to best preserve the original image structure. Under such an implementation mode, the SAHVF filter worked in a very similar way to those of detection-and-filtering structure, which has been widely and successfully used in impulse noise removal applications [28]–[30].

A practical way to detect whether the input noisy image contains only impulse noise corruption or not is worked with the additive noise estimation defined in Section III-A. For example,

according to the local approximately piece-smooth characteristic of the natural image structure [20], it is reasonable to assume that if the estimated additive noise deviation is very small (e.g., $\sigma_{n,1} \leq 5.0$), there should be only impulse noise corruption in the input noisy image.

VI. Simulation Results

The proposed filter structure has been extensively evaluated using a wide range of 512×512 24-bit RGB test images. Two standard quantitative measures are employed in the performance assessment. The *normalized mean square error* (NMSE) [17] measures the image distortion in the RGB color space. Let $\mathbf{s}(\mathbf{c})$ and $\mathbf{y}(\mathbf{c})$ denote the original and reconstructed pixel value at position $\mathbf{c} \in \mathbf{C}$, respectively, then

$$\mathrm{NMSE} = \frac{\sum_{\mathbf{c}\in\mathbf{C}} \|\mathbf{s}(\mathbf{c}) - \mathbf{y}(\mathbf{c})\|^2}{\sum_{\mathbf{c}\in\mathbf{C}} \|\mathbf{s}(\mathbf{c})\|^2}. \tag{30}$$

The *normalized color difference* (NCD) [17] measures the image distortion in the perceptual uniform CIELAB color space. It is given by

$$\mathrm{NCD} = \frac{\sum_{\mathbf{c}\in\mathbf{C}} \|\triangle E_{\mathrm{Lab}}(\mathbf{c})\|}{\sum_{\mathbf{c}\in\mathbf{C}} \|E_{\mathrm{Lab}}(\mathbf{c})\|} \tag{31}$$

where $\triangle E_{\mathrm{Lab}}(\mathbf{c})$ represents the difference between the original image pixel and its reconstruction at position $\mathbf{c}$ in the CIELAB color space, and $E_{\mathrm{Lab}}(\mathbf{c})$ denotes the original image pixel value in the CIELAB color space.

A. Additive Noise Suppression

The proposed SAHVF filter has been evaluated using natural RGB images contaminated by different types of additive noise and several noise contamination levels. Three group of reference filters were engaged in the restoration performance comparison, which include standard vector filters such as the VMF [4], the general VDF (GVDF) [5], and the AHF [13]; classic local statistics filters, such as the arithmetic mean filter and the 3-D LLSF given in (10); state-of-the-art adaptive vector filters, such as the ANNF [7]; and the multiple window configuration (MWC) filter [29].

1) Different Additive Noise Level: We first compared the performance of restoring natural color images contaminated by different levels of additive *Gaussian* noise. *Gaussian* noise was generated according to the PDF function given by (3), with the standard deviation σ set to 10, 20, 25, and 30 corresponding to four different noise levels. The window dimension of all reference filters and the presmoothing of the SAHVF was set to 3×3 for noise with $\sigma = 10$ to preserve the image structure, while for noise with $\sigma = 20, 25, 30$, it was set to 5×5 to achieve adequate smoothing. For the MWC, a recursive 3×3 filter structure was used for all noise levels as defined by [29]. The hybrid filtering window of the SAHVF was adaptive according to the detected structure activity value following the mechanism defined in Table II.

Fig. 3 shows the results with the 512×512-pixel 24-bit RGB color image *Lena* corrupted by different levels of *Gaussian* noise. The Mean filter and the ANNF performed significantly better than classic nonlinear filters, e.g., the VMF, the GVDF, and the AHF, from all levels of noise corruptions. The MWC filter with a recursive 3×3 window achieved a satisfactory result for low-*Gaussian* noise corruption. However, its performance was inferior to those of the ANNF and the 3-D-LLSF filter with a large window when $\sigma > 20$. Thanks to its flexible structure and window adaption, the proposed SAHVF has achieved a significant improvement over the ANNF, the MWC filter, and the 3-D-LLSF, with a more robust performance over all different noise levels.

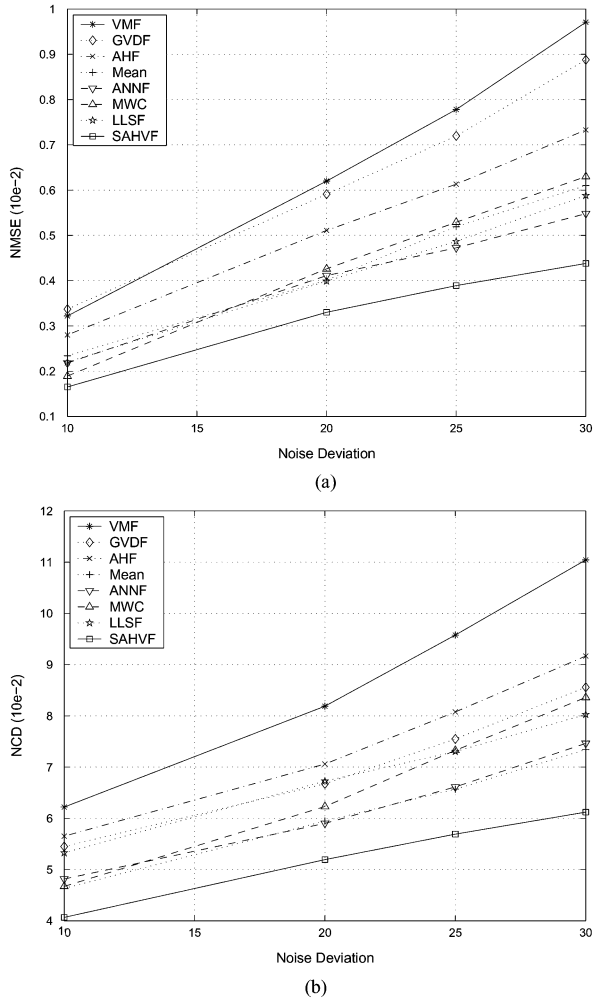

Fig. 3. Performance of various filters on restoration of the image *Lena* contaminated different levels of *Gaussian* noise. (a) The output distortion measured in *NMSE*. (b) The output distortion measured in NCD.

Fig. 4 presents the central part of the *Lena* corrupted by the *Gaussian* noise with $\sigma = 30$ and restored by various vector filters. The image detail structures were over-smoothed by the ANNF. Noises and large residues remained around edges and fine structures of the 3-D-LLSF output. Unpleasant color distortions were observed from the MWC output. The perceptual image quality of the SAHVF reconstruction was well recognized, where most of the fine image structures were well preserved and the flat areas restored were quite smooth in color perception.

2) Different Types of Additive Noise: In this experiment, three different types of additive noise, the *Gaussian* noise, the *Laplacian* noise, and the *uniform* noise, were used to corrupt test color images. All of them had the same standard deviation

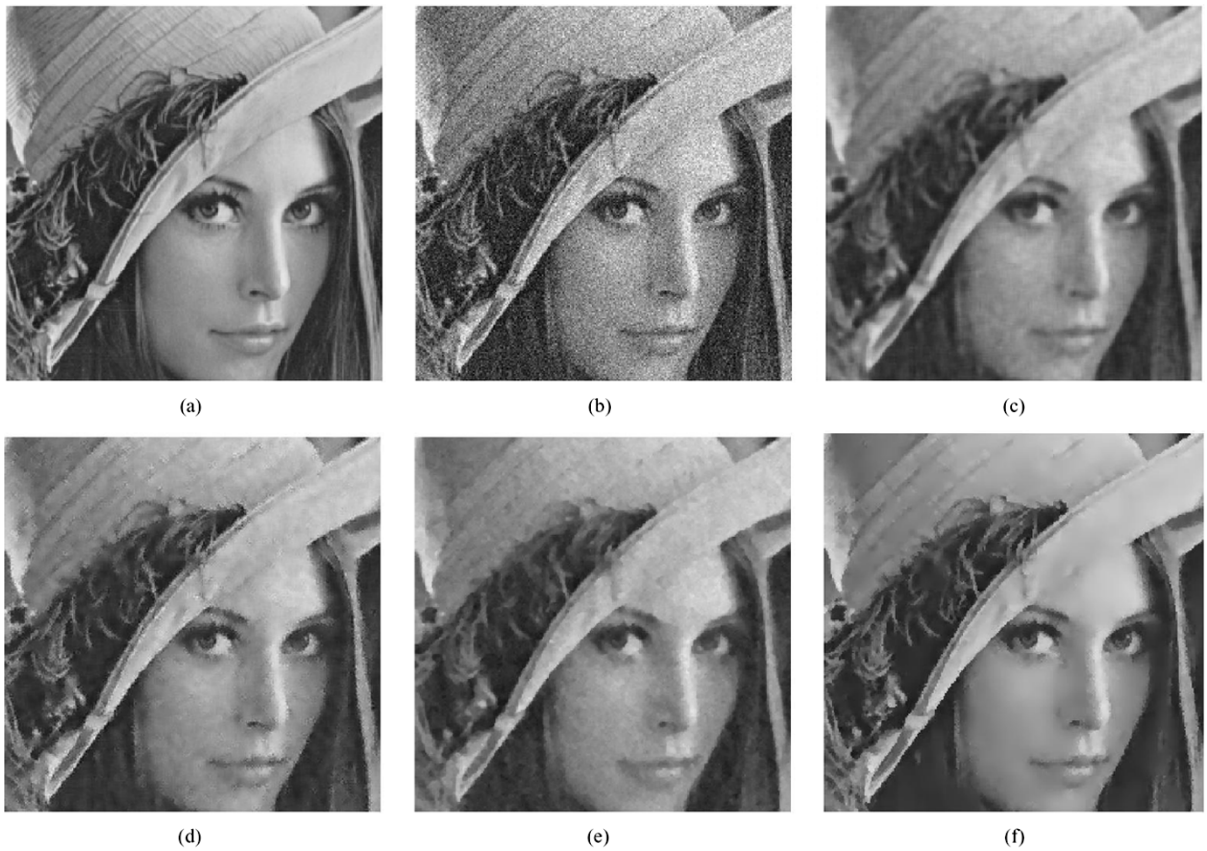

Fig. 4. Reconstruction of various filters for the image *Lena* corrupted by *Gaussian* noise with $\sigma = 30$. (a) The original image *Lena* (b) corrupted by *Gaussian* noise with $\sigma = 30$. (c) Output of the 5×5 ANNF filter. (d) Output of the 5×5 LLSF [three-dimensional (3-D)] filter. (e) Output of the MWC filter. (f) Output of the SAHVF filter.

$\sigma = 30$, and named as GN30, LN30, and UN30, respectively. The window dimension for all reference filters was set to 5×5 (except the MWC filter which used the recursive 3×3 filter structure). The presmoothing window of the SAHVF filter was preset to 5×5, whilst its hybrid filtering window was adaptive according to the structure activity.

Fig. 5 demonstrates the performance of different filters with 720×576-pixel 24-bit RGB color image *Barbara*. The AHF, the ANNF, and the MWC filter have achieved significant improvement over classic nonlinear filters for all types of additive noise. Nevertheless, their performances are still not comparable to the 3-D LLSF for the *Gaussian* and the *uniform* noises. The performance of the Mean filter and the 3-D LLSF degrade dramatically when the noise shifts from the short-tailed *uniform* or *Gaussian* distribution to the heavy-tailed *Laplacian* distribution. A better result is achieved by the proposed SAVHF, which is highly robust for heavy-tailed noises, sensitive to noise removal in fine structures, and efficient for smoothing color distortion in flat areas. Fig. 6 presents the reconstructed image details for the *Barbara* corrupted by *Laplacian* noise with $\sigma = 30$. The proposed SAHVF provides a more desirable reconstruction compared to the 3-D-LLSF and the MWC, with smoother backgrounds, clearer texture and shaper image structures.

B. Impulse Noise Removal

Two types of impulse noise, the *PS* impulse that has a fixed value from $\{0, 255\}$ and the *random* impulse which follows the random distribution in [0, 255], were generated to corrupt test images by the channel-correlated method stated in Section II–A, i.e., an independent intra channel corruption followed by a 50% interchannel error correlation. Seveal vector filters were included in the experiment, which were the VMF [4], the DDF [6], the HF [13], the PGF [25], the vector SD-ROM (VROM) filter [31], the MWC filter [29], and the self-adaptive algorithm for impulsive noise reduction (SAINR) filter [30]. In all of the cases, the filter window size is set to 3×3. The threshold for the PGF and the VROM filter are tuned individually to obtain their best performance for each restoration case.

Fig. 7 shows some results of restoring the 512×512-pixel 24-bit RGB color image *peppers*, where the image is corrupted by *PS* impulse as well as *random* impulse, with the noise ratio p ranging from 5% to 30%. The SAHVF renders a comparable top performance to the PGF when the noise ratio is very low, while performing impressively better than the PGF when the noise ratio is higher than 10%. For highly corrupted images, the performance difference between the SAHVF and the high-ranked MWC filter is always negligible. Compared to the computation intensive offline parameter training required by the MWC filter, the SAHVF only requires a few empirically determined parameters, which is quite a saving in terms of computational costs. It needs to be noted that the restoration results when noise ratio $p < 5\%$ or $p > 30\%$, although not shown in the current figure, have demonstrated a very similar trend in the experiments.

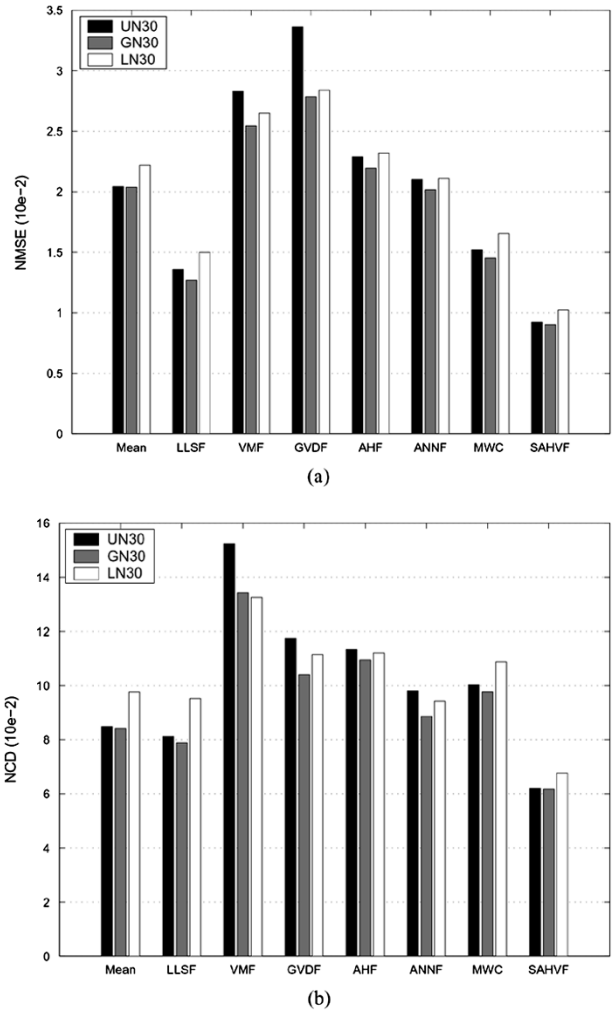

Fig. 5. Performance of various filters on restoration of the image *Barbara* contaminated by different types of additive noise. (a) The output distortion measured in NMSE. (b) The output distortion measured in NCD.

TABLE III
RESULTS OF VARIOUS FILTERS ON RESTORATION OF RGB NATURAL IMAGES CONTAMINATED BY DIFFERENT LEVELS OF MIXED NOISE. (a) *LENA* WITH DIFFERENT LEVELS OF MIXED NOISE (10^{-2}). (b) *BARBARA* WITH DIFFERENT LEVELS OF MIXED NOISE (10^{-2})

(a) *Lena* with different levels of mixed noise (10^{-2})

Filter	*G15I15*		*G30I10*	
	NMSE	*NCD*	*NMSE*	*NCD*
GVDF [5]	0.4530	5.6346	0.8444	8.4812
AHF [13]	0.4465	6.2048	0.8432	9.7188
ANNF [7]	0.3762	5.2868	0.5869	7.6823
CBANNF [10]	0.3843	5.3152	0.6407	7.7733
PGF [25]	0.4519	6.5259	0.9669	11.7726
MWC [29]	0.3311	5.0310	0.6018	7.5766
SAHVF	0.2628	4.4253	0.5002	6.9381

(b) *Barbara* with different levels of mixed noise (10^{-2})

Filter	*G15I15*		*G30I10*	
	NMSE	*NCD*	*NMSE*	*NCD*
GVDF [5]	2.2020	7.3431	2.9367	10.7166
AHF [13]	1.9218	7.4006	2.3198	10.9442
ANNF [7]	1.8614	6.5323	2.0791	8.8663
CBANNF [10]	1.9542	6.7070	2.2857	9.3890
PGF [25]	1.3938	7.6165	2.7552	12.7332
MWC [29]	1.3010	7.0344	1.8622	8.6335
SAHVF	0.8215	5.6624	1.2332	7.3943

TABLE IV
COMPUTATION COMPLEXITY ANALYSIS OF SOME PARTS OF THE SAHVF FILTER

Parts	VMF	Noise Est.	Pre-smoothing	Classification	MPF	ANNF	SWAF
ADDS	$O(N^4)$	$O(N^2)$	$O(N^2)$	$O(N^2)$	$O(N^2)$	$O(N^4)$	$O(N^2)$
MULTS	–	$O(N^2)$	$O(N^2)$	$O(N^2)$	$O(N^2)$	$O(N^4)$	$O(N^2)$
SQRTS	$O(N^4)$	–	–	–	$O(N^2)$	$O(N^4)$	–
COMPS	$O(N^2)$	–	–	$O(N^2)$	$O(N^2)$	$O(N^4)$	–

C. Mixed-Noise Suppression

Two different levels of *mixed* noises, *G15I5* and *G30I10*, are used in this experiment to contaminate the test color images. The *G15I5* was mixed by *Gaussian* noise with $\sigma = 15$ and *random* impulse noise with $p = 5\%$, while *G30I10* was mixed by *Gaussian* noise with $\sigma = 30$ and *random* impulse with $p = 10\%$. Several robust vector filters were also employed in the experiment, including the GVDF [5], the AHF [13], the ANNF, the CBANNF [10], the PGF, and the MWC filter. The preset window sizes are 3×3 for *G15I5* and 5×5 for *G30I10*, respectively. The MWC used a recursive 3×3 window all over the experiment, and the hybrid filtering window of the SAHVF was adaptive according to the detected structure activity value following the mechanism defined in Table II.

Table III briefly summaries the restoration results for all the tested filters on two 24-bit RGB color images, *Lena* and *Barbara*. Although the PGF and the MWC filter provide reasonable NMSE values at low levels of mixed noise, its NCDs and perceptual image quality are far worse than those of the SAHVF. For serious mixed-noise contamination, the SHAVF performs significantly better than the rest of filters, such as the ANNF or the MWC. The reconstructions by the SAHVF, although not shown in this paper due to the page limitation, have desirable subjective qualities in terms of chromatic retention and image detail preservation.

D. Implementation Complexity Analysis

A general framework to evaluate the computational requirements of image filtering algorithms has been formulated in [30], [32], and [33]. In this framework, the computational complexity of a specific filter is assumed to be the total time to complete an operation for a given $N \times N$ symmetric window, which contains N^2 vector sample of order $p(\mathcal{R}^p)$, e.g., $p = 3$ for color image processing. Four elementary operations are taken into account in the analysis, which include additions (ADDS), multiplications (MULTS), square roots (SQRTS), and comparisons (COMPS).

Table IV presents the elementary operations required for most parts of the SAHVF filter, where the Euclidian distance is employed as the distance measure. The computation complexity of the SAHVF still seems fairly reasonable despite of its complicated system structure. The operations involved in the noise estimation, presmoothing, and classification are only of $O(N^2)$ on the pixel basis, while a classic VMF requires a computation cost of $O(N^4)$ on the pixel basis. Its subfilters, such as the MPF

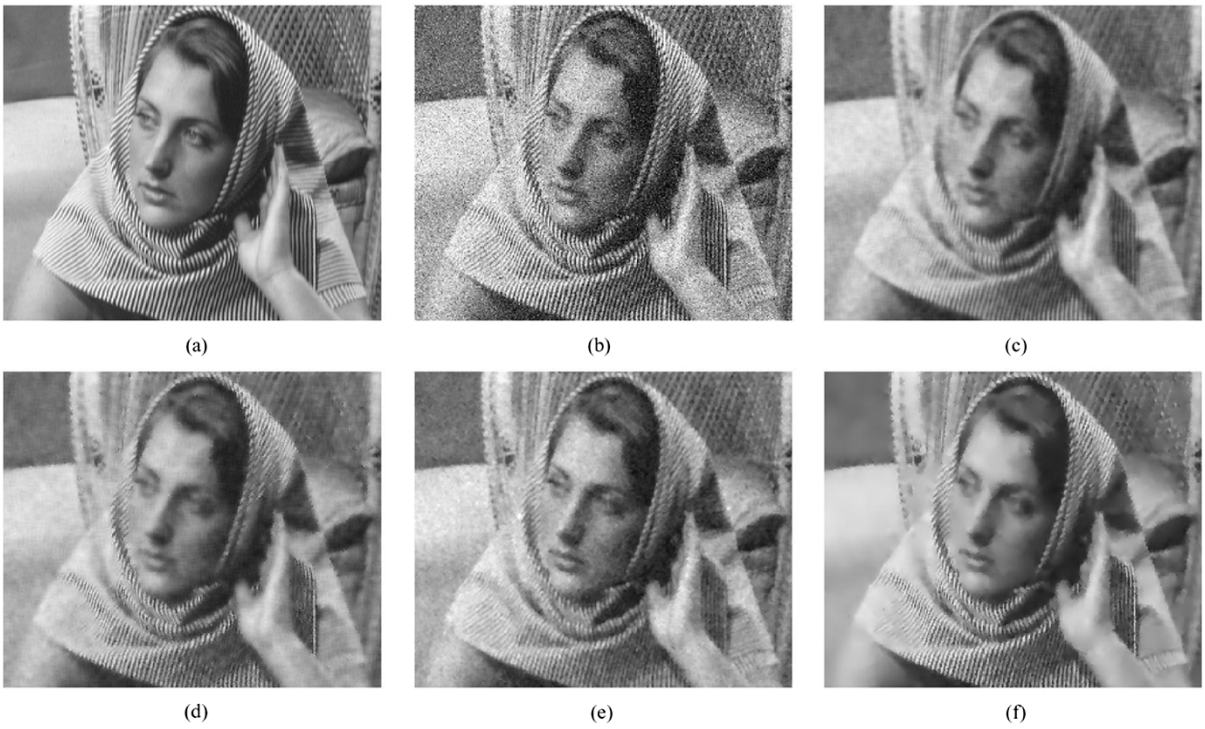

Fig. 6. Reconstruction of various filters for the image *Barbara* corrupted by *Laplacian* noise with $\sigma = 30$.(a) The original image *Barbara* (b) corrupted by *Laplacian* noise with $\sigma = 30$. (c) Output of the 5×5 ANNF filter. (d) Output of the 5×5 LLSF (3-D) filter. (e) Output of the MWC filter. (f) Output of the SAHVF filter.

TABLE V
COMPUTER TIMES OF THE SAHVF AND OTHER FILTERS WITH DIFFERENT WINDOW SIZE AND WORK MODES, WHERE TIME IS EXPRESSED IN SECONDS

Window size	VMF	AHF	ANNF	PGF	LLSF	SAHVF
3×3	10.2	21.1	16.9	10.1	16.3	20.0 [a]/ 46.1
5×5	67.5	149.6	124.2	38.3	20.0	53.7

[a] impulse noise mode, noise estimation and pre-processing are switched off, the filter worked in the detection-and-filtering mode with the MPF and ANNF filter only.

and the SWAF, are also very computation efficient compared to the VMF and the ANNF, as they require only $O(N^2)$ order of computation cost on the pixel basis. Computation complexity of the quadtree decomposition has been analyzed in [34] which is reasonable. The color space transform between the RGB and the YC_bC_r possesses very efficient fast implementations.

Table V shows the computation time recorded on the same simulation platform (P4 2.0 GHz/512 MB DDR/Window XP) with the RGB image *Peppers* corrupted by the mixed-noise *G15I5*. Two window dimensions, 3×3 and 5×5, are used for reference filters and the presmoothing of the SAHVF filter. For the 3×3 window size, two work modes of the SAHVF filter, i.e., the impulse noise mode and the default mode, are tested and presented their results side by side. It is interesting that the computation cost of SAHVF filter under impulse noise mode is just a slightly worse than the ANNF, comparable to the AHF filter. When window size increases from 3×3 to 5×5, which is often used for restoration of moderate additive noise corruption, the computation time of the SAHVF increases just around 20% (under normal modes), while implementing the computation time of most other nonlinear filters increased dramatically. Some filters, such as the AHF and the ANNF, even required twice the time of the SAHVF to process the same image.

VII. CONCLUSION

In this paper, various noise types in digital color imaging are reviewed. Based on the human visual perception, a structure-adaptive filter named SAHVF is proposed for color image restoration. The filter includes a noise-adaptive structure activity classification, which provides a robust structure activity detection and partition for each pixel position. The results of the classification are utilized by a switch-based hybrid filtering structure, which is able to select an optimal subfiltering and processing window to provide the best tradeoff between noise suppression and visual quality.

The proposed SAHVF filter has demonstrated a robust performance in suppressing different types of noise contamination. For additive noise contamination, it can produce a reconstruction with smoother background and sharp texture, which is significantly better in perceived image quality. For impulse noise corruption, the filter provides a comparable performance to the state-of-the-art filters in noise removal and structure preservation. Beside it robust performance, the filter demands a moderate computation cost for most restoration applications, especially for high-corrupted color images, the SAHVF can provide a better reconstruction, with less than half of the processing time than those classic vector filters.

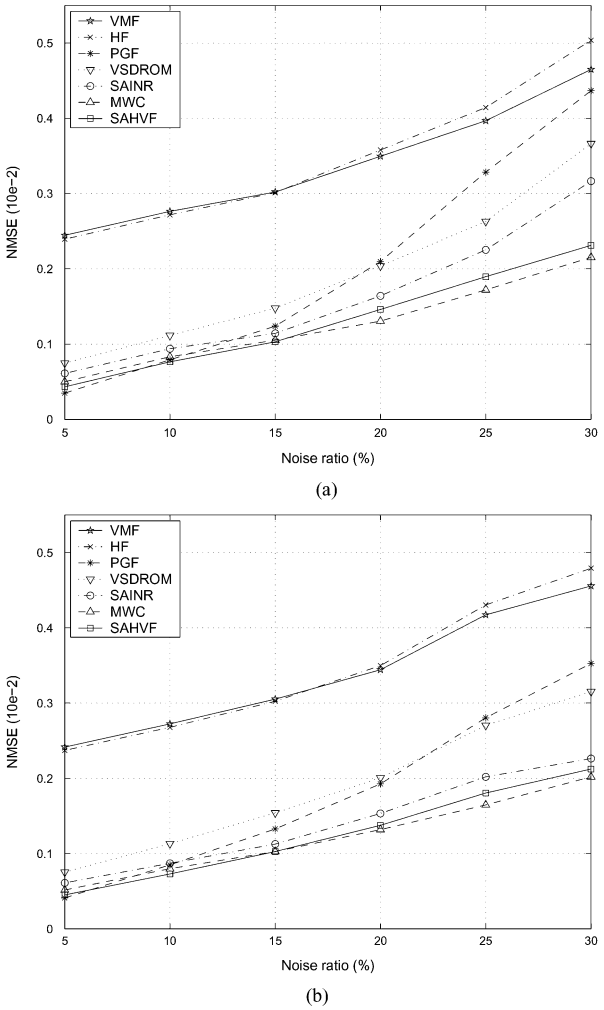

Fig. 7. Performance of various filters on restoration of the image *Peppers* contaminated different impulse noises. (a) PS impulse noise. (b) Random impulse noise.

ACKNOWLEDGMENT

The authors would like to thank the anonymous reviewers for their valuable comments that help to improve the paper.

REFERENCES

[1] V. Barnett, "The ordering of multivariate data," *J. Stat. Soc. Amer. A.*, vol. 139, no. 3, pp. 318–354, 1976.

[2] I. Pitas and P. Tsakalides, "Multivariate ordering in color image filtering," *IEEE Trans. Circuits Syst. Video Technol.*, vol. 1, no. 3, pp. 247–259, Sep. 1991.

[3] R. C. Hardie and G. R. Arce, "Ranking in R^p and its use in multivariate image estimation," *IEEE Trans. Circuits Syst. Video Technol.*, vol. 1, no. 2, pp. 197–209, Jun. 1991.

[4] J. Astola, P. Haavisto, and Y. Neuov, "Vector median filter," *Proc. IEEE*, vol. 78, no. 4, pp. 678–689, Apr. 1990.

[5] P. E. Trahanias and A. N. Venetsanopoulos, "Vector directional filters: A new class of multichannel image processing filter," *IEEE Trans. Image Process.*, vol. 2, no. 4, pp. 5288–534, Apr. 1993.

[6] D. G. Karakos and P. E. Trahania, "Combining vector median and vector directional filters: the directional-distance filter," in *Proc. IEEE Int. Conf. Image Processing*, vol. 1, Washington, DC, Oct. 1995, pp. 171–174.

[7] K. N. Plataniotis, S. Vinayagamoorthy, D. Androutsos, and A. N. Venetsanopoulos, "An adaptive nearest neighbor multichannel filter," *IEEE Trans. Circuits Syst. Video Technol.*, vol. 6, no. 6, pp. 699–703, Dec. 1996.

[8] K. N. Plataniotis, D. Androutsos, and A. N. Venetsanopoulos, "Adaptive multichannel filters for color image processing," *Signal Process.: Image Commun.*, vol. 11, no. 3, pp. 171–177, Jan. 1998.

[9] ——, "Color image processing using adaptive vector directional filters," *IEEE Trans. Circuits Syst. II, Exp. Briefs*, vol. 45, no. 10, pp. 1414–1419, Oct. 1998.

[10] ——, "Adaptive fuzzy systems for multichannel signal processing," *Proc. IEEE*, vol. 87, no. 9, pp. 1601–1622, Sep. 1999.

[11] E. S. Hore, B. Qiu, and H. R. Wu, "Improved color image vector filtering using fuzzy noise detection," *Opt. Eng.*, vol. 42, no. 6, pp. 1656–1664, Jun. 2003.

[12] K. Tang, J. Astola, and Y. Neuvo, "Nonlinear multivariate image filtering techniques," *IEEE Trans. Image Process.*, vol. 4, no. 6, pp. 788–798, Jun. 1995.

[13] M. Gabbouj and F. A. Cheikh, "Vector median-vector directional hybrid filter for color image restoration," in *Proc. EUSIPCO*, vol. 2, Trieste, Italy, Sep. 10–13, 1996, pp. 879–881.

[14] L. Khriji and M. Gabbouj, "Vector median-rational hybrid filters for mutichannel image processing," *IEEE Signal Process. Lett.*, vol. 6, no. 8, pp. 186–190, Aug. 1999.

[15] Y. H. Lee and S. A. Kassam, "Generalized median filtering and related nonlinear filtering techniques," *IEEE Trans. Acoust., Speech, Signal Process.*, vol. ASSP-33, no. 3, pp. 672–683, Jun. 1985.

[16] W. K. Pratt, Ed., *Digital Image Processing*. New York: Wiley, 1991.

[17] K. N. Plataniotis and A. N. Venetsanopoulos, Eds., *Color Image Processing and Applications*. Berlin, Germany: Springer, 2000.

[18] J. Astola and P. Kuosmanen, Eds., *Fundamentals of Nolinear Digital Filtering*. Boca Raton, FL: CRC, 1997.

[19] J. S. Lee, "Digital image enhancement and noise filtering by use of local statistics," *IEEE Trans. Pattern Anal. Mach. Intell.*, vol. PAMI-2, no. 2, pp. 165–168, Feb. 1980.

[20] A. Jain, Ed., *Fundamentals of Digital Image Processing*. Englewood Cliffs, NJ: Prentice-Hall, 1989.

[21] J. Immerker, "Fast noise variance estimation," *Comput. Vis. Image Understand.*, vol. 64, no. 2, pp. 300–302, Sep. 1996.

[22] L. Yin, R. Yang, M. Gabbouj, and Y. Neuvo, "Weighted median filters: A tutorial," *IEEE Trans. Circuits Syst. II, Exp. Briefs*, vol. 43, no. 3, pp. 157–191, Mar. 1996.

[23] M. Kamel, C. T. Sun, and L. Guan, "Image compression by variable block truncation coding with optimal threshold," *IEEE Trans. Signal Process.*, vol. 39, no. 1, pp. 208–212, Jan. 1991.

[24] H.-L. Eng and K.-K. Ma, "Noise adaptive soft-switching median filter," *IEEE Trans. Image Process.*, vol. 10, no. 2, pp. 242–251, Feb. 2001.

[25] C. Kenney, Y. Deng, B. S. Manjunath, and G. Hewer, "Peer group image enhancement," *IEEE Trans. Image Process.*, vol. 6, no. 2, pp. 326–334, Feb. 2001.

[26] R. O. Duda and P. E. Hart, Eds., *Pattern Classification and Scene Analysi*. New York: Wiley, 1973.

[27] J. S. Lim, Ed., *Two-Dimensional Signal and Image Processing*. Englewood Cliffs, NJ: Prentice-Hall, 1990.

[28] I. Pitas and A. N. Venetsanopoulos, Eds., *Nonlinear Digital Filters: Principles and Application*. Norwell, MA: Kluwer, 1990.

[29] E. S. Hore, B. Qiu, and H. R. Wu, "Prediction based image restoration using a multiple window configuration," *Opt. Eng.*, vol. 41, no. 8, pp. 1–11, Aug. 2002.

[30] B. Smolka, A. Chydzinski, K. Wojciechowski, K. N. Plataniotis, and A. N. Venetsanopoulos, "Self-adaptive algorithm for impulsive noise reduction in color images," *Pattern Recognit.*, vol. 35, no. 8, pp. 1771–1784, 2002.

[31] M. S. Moore, M. Gabbouj, and S. K. Mitra, "Vector SD-ROM filter for removal of impulse noise from color images," in *Proc. EURASIP Conf. DSP for Multimedia Communication and Services*, Krakow, Poland, Jun. 24–26, 1999.

[32] *Color Image Processing Handbook*, S. J. Sangwine and R. E. N. Horner, Eds., Chapman & Hall, London, 1998, pp. 188–209.

[33] M. Barni and V. Cappellini, "On the computational complexity of multivariate median filters," *Signal Process.*, vol. 71, pp. 45–54, 1998.

[34] R. Shukla, P. L. Dragotti, M. Do, and M. Vetterli, "Improved quadtree algorithm based on joint coding for piecewise smooth image compression," in *Proc. IEEE Int. Conf. Multimedia and Expo.*, vol. 1, Aug. 2002, pp. 26–29.

Zhonghua Ma (M'02) was born in Zhejiang, China, in 1973. He received the B.Eng. degree from Shanghai Jiaotong University, China, the M.Eng. degree from the Dalian University of Technology, China, in 1995 and 1999, respectively, and the Ph.D. degree in communications and information systems from Shanghai Jiaotong University, China, in 2002.

From 2002 to 2004, he was a Research Fellow conducting an Australia Research Council (ARC) funded project with the School of Computer Science and Software Engineering, Monash University, Melbourne, Australia. He is currently with the School of Information Technologies, University of Sydney, Australia. His research interests include multivariance signal processing, color image restoration, video compression, and robust streaming.

Hong Ren Wu was born in Beijing, China, in 1956. He received the B.Eng. and M.Eng. degrees from the University of Science and Technology (formerly Beijing University of Iron and Steel Technology), Beijing, in 1982 and 1985, respectively, and the Ph.D. degree in electrical and computer engineering from the University of Wollongong, Wollongong, Australia, in 1990.

From 1982 to 1985, he was an Assistant Lecturer with the Department of Industrial Automation, University of Science and Technology. He joined the Department of Robotics and Digital Technology, Chisholm Institute of Technology, as a Lecturer in 1990. From 1990 to January 2005, he was on the academic staff of the Faculty of Information Technology, Monash University, Melbourne, Australia, where he was last an Associate Professor. He joined the School of Electrical and Computer Engineering, Royal Melbourne Institute of Technology, where he is currently a Professor of visual communications engineering and Discipline Head of software and networks. Since 1987, he has participated in and headed numerous research projects and industrial contracts in the fields of signal processing, image processing, and digital video coding compression and transmission, including picture quality assessment and perceptual coding.

Bin Qiu (M'93–SM'00) received the Ph.D. degree from the University of Manchester Institute of Science and Technology, Manchester, U.K., in 1989.

He is currently an Associate Professor with the School of Computer Science and Software Engineering, Monash University, Melbourne, Australia. He has conducted research in algorithms and applications of intelligent signal processing in communication networks, image processing, and video processing.